Characterization of Large Peptide Fragments Derived from the N-Terminal Domain of the Ribosomal Protein L9: Definition of the Minimum Folding Motif and Characterization of Local El...

ARTICLE *in* BIOCHEMISTRY · DECEMBER 2002

Impact Factor: 3.02 · DOI: 10.1021/bi026410c · Source: PubMed

5 AUTHORS, INCLUDING:

Jia-Cherng Horng
National Tsing Hua University
44 PUBLICATIONS **797** CITATIONS
SEE PROFILE

Robert Fairman
Haverford College
78 PUBLICATIONS **3,733** CITATIONS
SEE PROFILE

Characterization of Large Peptide Fragments Derived from the N-Terminal Domain of the Ribosomal Protein L9: Definition of the Minimum Folding Motif and Characterization of Local Electrostatic Interactions†

Jia-Cherng Horng,‡ Viktor Moroz,‡ Daniel J. Rigotti,§ Robert Fairman,§ and Daniel P. Raleigh*,‡,||

Department of Chemistry, State University of New York at Stony Brook, Stony Brook, New York 11794-3400, Graduate Program in Biophysics, Graduate Program in Molecular and Cellular Biology, and Graduate Program in Biochemistry and Structural Biology, State University of New York at Stony Brook, Stony Brook, New York 11794, and Department of Molecular, Cell and Developmental Biology, Haverford College, Haverford, Pennsylvania 19041

Received July 4, 2002; Revised Manuscript Received August 30, 2002

ABSTRACT: A set of peptides derived from the N-terminal domain of the ribosomal protein L9 (NTL9) have been characterized in an effort to define the minimum unit of this domain required to fold and to provide model peptides for the analysis of electrostatic interactions in the unfolded state. NTL9 is a 56-residue α−β protein with a β1−loop−β2−α1−β3−α2 topology. The β-sheet together with the first helix comprise a simple example of a common supersecondary motif called the split β−α−β fold. Peptides corresponding to the β1−loop−β2 unit are unstructured even when constrained by an introduced disulfide. The pK_as of Asp-8 and Glu-17 in these peptides are slightly lower than the values found for shorter peptides but are considerably higher than the values in NTL9. A 34-residue peptide, which represents the β1−loop−β2−α1 portion of NTL9, is also unstructured. In contrast, a 39-residue peptide corresponding to the entire split β−α−β motif is folded and monomeric as judged by near- and far-UV CD, two-dimensional NMR, ANS binding experiments, pK_a measurements, and analytical ultracentrifugation. The fold is very similar to the structure of this region in the intact protein. Thermal and urea unfolding experiments show that it is cooperatively folded with a $\Delta G°$ of unfolding of 1.8−2.0 kcal/mol and a T_m of 58 °C. This peptide represents the first demonstration of the independent folding of an isolated split β−α−β motif, and is one of only four naturally occurring sequences of fewer than 40 residues that has been shown to fold cooperatively in the absence of disulfides or ligand binding.

The N-terminal domain of the ribosomal protein L9 (NTL9)[1] forms a small, cooperatively folded, mixed α−β structure (Figure 1). It lacks disulfides and does not require a cofactor or metal ion binding to fold, making it an attractive system for studies of protein folding and stability. Detailed investigations have shown that it folds rapidly in a two-state fashion under a very wide range of conditions (*1*−*3*). The protein consists of a three-stranded antiparallel β-sheet flanked by two α-helices, the second of which extends to form the interdomain connector in the intact protein (*4*−*6*). The three-stranded sheet and the first helix comprise the first

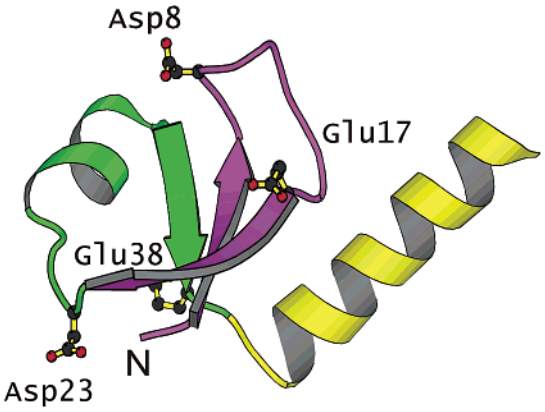

FIGURE 1: Ribbon diagram of the N-terminal domain of ribosomal protein L9. This figure was made using the program Molscript (*47*). The purple portion denotes the region of residues 1−22 and the green portion the region of residues 23−39, and the C-terminal helix, residues 40−56, is colored yellow. Acidic residues in the region of residues 1−39 are indicated, and the N-terminus is labeled.

† Supported by NSF Grant MCB-0079406 to D.P.R.

* To whom correspondence should be addressed. E-mail: draleigh@notes.cc.sunysb.edu. Phone: (631) 632-9547. Fax: (631) 632-7960.

‡ Department of Chemistry, State University of New York at Stony Brook.

§ Haverford College.

|| Graduate Program in Biophysics, Graduate Program in Molecular and Cellular Biology, and Graduate Program in Biochemistry and Structural Biology, State University of New York at Stony Brook.

[1] Abbreviations: ANS, 1-anilinonaphthalene 8-sulfonate; CD, circular dichroism; CG(1−22)GC$_{ox}$, 26-residue peptide corresponding to residues 1−22 of L9 with a CG dipeptide at the N-terminus and a GC dipeptide at the C-terminus (the subscript ox refers to the oxidized version of the peptide with an intact disulfide); FMOC, *N*-9-fluorenylmethyloxycarbonyl; HBTU, *O*-benzotriazole-*N*,*N*,*N*′,*N*′-tetramethyluronium hexafluorophosphate; HPLC, high-pressure liquid chromatography; NMR, nuclear magnetic resonance; NOESY, nuclear Overhauser effect spectroscopy; NTL9, N-terminal domain of ribosomal protein L9 from *B. stearothermophilus*; NTL9$_{1-39}$, peptide with an amidated C-terminus corresponding to the first 39 residues of the ribosomal protein L9 from *B. stearothermophilus*; NTL9$_{1-22}$, peptide with an amidated C-terminus corresponding to the first 22 residues of the ribosomal protein L9 from *B. stearothermophilus*; PAL, polystyrene FMOC support for peptide amides; ROESY, rotating frame nuclear Overhauser effect spectroscopy; TOCSY, total correlation spectroscopy; TSP, sodium 3-trimethylsilyl-2,2,3,3-d_4 propionate.

10.1021/bi026410c CCC: $22.00
Published on Web 10/15/2002

39 residues of the domain and form what is the smallest and probably the simplest example of a common supersecondary motif called the split $\beta-\alpha-\beta$ fold or ABCD motif (*7*−*9*). This region of the protein consists of the segments colored purple and green in Figure 1. The split $\beta-\alpha-\beta$ motif is found as substructure in a large number of proteins, but there are no published reports that indicate if it is capable of folding in isolation.

Considerable recent work has been devoted to developing small stably folded "miniproteins" both by de novo design and by modification and minimization of natural proteins (*10*−*17*). Particularly interesting are small systems that do not require disulfides or cofactor binding to fold. Such molecules are emerging as popular model systems for computational, theoretical, and experimental studies of protein folding and protein stability (*18*−*20*). Small proteins can also be exploited to provide well-defined structural scaffolds for the presentation of peptide libraries (*21*−*23*). To date, almost all well-characterized small proteins either are all helical or have other simple folds such as small β-meanders (the WW domains) or zinc finger-derived β-hairpin helix units (*24*−*26*). The split $\beta-\alpha-\beta$ structure with its Greek keylike arrangement of elements of secondary structure is more complex than these.

Here we report the synthesis and biophysical characterization of a set of large peptide fragments derived from NTL9 and demonstrate that a 39-residue peptide corresponding to the split $\beta-\alpha-\beta$ motif is able to fold to a well-defined native state. In contrast, fragments which include just the first two β-strands and intervening loop do not fold even when constrained by a disulfide, nor does a 34-residue peptide which contains the strand−loop−strand unit as well as the first helix. This work thus defines the minimal elements of NTL9 required to fold and provides the first example of a $\beta-\alpha-\beta$ motif that can fold in isolation.

Analysis of the shorter fragments also provides information about local tendencies to form structure in the unfolded state. This is particularly interesting in the case of NTL9 since previous investigations have revealed the presence of nonrandom interactions in the unfolded state (*27*, *28*). Characterizing unfolded state interactions is a critical but difficult part of defining the folding process (*29*). Of most relevance to protein folding and protein stability is the nature of the denatured state under conditions which favor the native state. The high cooperativity of the folding process normally prevents direct observation of this state, and indirect approaches have to be used. Analysis of sets of small peptide fragments corresponding to individual elements of secondary structure is a standard method and provides information about local preferences in forming structure in the absence of tertiary interactions. Analyzing larger fragments such as those characterized here can extend these studies (*30*).

Studies of peptide fragments, while very useful, cannot provide a complete picture of the structural propensities of the unfolded state because they necessarily are unable to mimic interactions, which require the entire chain. pH-dependent studies of protein stability can provide information about these important interactions (*28*, *31*−*34*). Comparison of the experimentally determined pH dependence of the stability of a protein ($\Delta\Delta G°$) to the $\Delta\Delta G°$ values predicted by the Tanford linkage relationship forms the basis of the approach. The linkage relationship, which is exact, relates $\Delta\Delta G°$ to ΔQ, the difference in the number of protons bound to the folded and unfolded state. Knowledge of the pK_as of the folded and unfolded state is sufficient to define ΔQ. NTL9 is a particularly attractive protein for such studies since the native state is stable over a very large pH range and the unfolding transitions are two-state and reversible. There are six acidic residues in NTL9, and they are all well-separated and titrate independently. Information is obtained about the unfolded state by using the native state pK_a values of these residues together with model pK_a values for the unfolded state to construct theoretical stability versus pH curves. Comparison of the calculated and experimental stability versus pH curves provides a test of how well the model pK_a values capture unfolded state interactions. In our initial study, we modeled the unfolded state pK_as using a set of short peptide fragments. These fragments corresponded to the individual β-strands and helices and were designed to account for purely local sequence effects. We observed a significant deviation between the experimental and calculated plots of $\Delta\Delta G°$ versus pH, indicating that there were residual electrostatic interactions in the unfolded state that were not captured by our model peptides. The peptides analyzed here provide an alternative model of unfolded state pK_as. This could be particularly important for two of the acidic residues, Asp-8 and Glu-17, since they are located just before the start and just after the end of a segment rich in lysines, respectively. Our earlier study split this region into two peptides; thus, each of these acidic residues could interact with only a subset of the lysine residues.

MATERIALS AND METHODS

Peptide Synthesis and Purification. All of the peptides were synthesized on a 0.22 mmol scale by solid phase methods using FMOC-protected amino acids and HBTU-mediated coupling on Millipore 9050 Plus and Rainin PS-3 automated peptide synthesizers with standard reaction cycles. All β-branched amino acids and all residues coupling to β-branched amino acids were double coupled. Each coupling, except for the last, was followed by a capping step using acetic anhydride. Use of a resin with a PAL linker generated an amidated C-terminus following cleavage from the resin with a 91% trifluoroacetic acid (TFA)/3% anisole/3% thioanisole/3% ethanedithiol mixture. Each peptide has a free N-terminus. Reverse phase HPLC using a Vydac C_{18} semipreparative column was used to purify the peptides. H_2O/acetonitrile (ACN) gradients with 0.1% TFA as the counterion were used. The peptides are designated as follows: $NTL9_{1-22}$, the first 22 residues of NTL9; $NTL9_{1-34}$, the first 34 residues; $NTL9_{1-39}$, the first 39 residues and CG(1−22)GC which is the first 22 residues of NTL9 with a CG unit added to the N-terminus and a GC unit added to the C-terminus. The $NTL9_{1-22}$, CG(1−22)GC, $NTL9_{1-34}$, and $NTL9_{1-39}$ fragments eluted at 24, 25, 30, and 33% acetonitrile, respectively. The identities of all peptides were confirmed by using matrix-assisted laser desorption ionization time-of-flight (MALDI-TOF) mass spectroscopy. The calculated and observed molecular weights were as follows: $NTL9_{1-22}$, calculated 2430.1, observed 2429.6; CG(1−22)GC, calculated 2750.5, observed 2753.4; $NTL9_{1-34}$, calculated 3785.6, observed 3794.7; and $NTL9_{1-39}$, calculated 4283.2, observed 4284.9.

Formation of the Disulfide in CG(1−22)GC. The reduced CG(1−22)GC peptide was first dissolved in a 3 M guanidine hydrochloride (GuHCl) solution (pH 1.85) to inhibit any aggregation and intermolecular disulfide formation. Then, oxidation of the reduced peptides was carried out in a 0.2 M tris(hydroxymethyl)aminomethane buffer at pH 8.5 for 6 h before separation on a semipreparative Vydac C18 reverse phase HPLC column. The final GuHCl and peptide concentrations in the reaction mixture were 0.3 M and ∼1 mM. The identity of the purified peptide was confirmed by mass spectroscopy.

Circular Dichroism (CD) Spectroscopy. All CD experiments were performed using Aviv model 62A DS and 202SF circular dichroism spectrometers. All measurements were performed in the 10 mM phosphate and 100 mM NaCl buffer (pH 5.4) at 25 °C. These conditions were chosen to match our studies of intact NTL9. Additional experiments were performed in 400 mM Na_2SO_4 at pH 5.4. The peptide concentration was 20−40 μM for far-UV experiments. Far-UV wavelength scans were performed in a 1 mm quartz cuvette using five repeats with an averaging time of 3 s at each wavelength and a spectrometer bandwidth of 1.5 nm. Urea-induced denaturation was performed in a 1 cm cuvette by monitoring the signal at 222 nm. Samples for near-UV measurements were 300 μM. A 1 cm quartz cuvette was used for near-UV measurements and the thermal unfolding experiment. The thermal unfolding curve was monitored at 280 nm. Protein and peptide concentrations were determined from absorbance measurements using the method of Pace and coworkers (*35*).

Fluorescence. The fluorescence emission signal was collected at 25 °C using an ISA Fluorolog spectrometer. The unfolding transition curve of the $NTL9_{1-39}$ fragment was determined by monitoring the emission signal change of Tyr-25 at 305 nm. The sample concentration for the fluorescence experiment was 20 μM, and the same buffer conditions as in the CD experiments were used. The ANS (1-anilinonaphthalene-8-sulfonate) fluorescence was measured using 2 μM ANS and 4 μM peptide. The ANS binding experiments were performed using an excitation wavelength of 370 nm, and emission spectra were recorded over the range of 380−650 nm. The concentration of the ANS stock solution was determined using a molar absorption coefficient of 7.8×10^3 M^{-1} cm^{-1} at 372 nm in methanol (provided by Molecular Probes).

Urea and Thermal Denaturation Curve Fitting. Urea denaturation curves were fit using standard methods (*36*). A two-state model was used to fit data collected from CD and fluorescence experiments to determine the stability of $NTL9_{1-39}$, $\Delta G_U°(H_2O)$, in the absence of urea. The free energy of unfolding is assumed to be a linear function of denaturant concentration.

$$\Delta G_U° = \Delta G_U°(H_2O) - m[\text{urea}] \quad (1)$$

where $\Delta G_U°$ is the apparent free energy for the N to D transition. Thermal unfolding data for $NTL9_{1-39}$ were fit as described previously (*2*). However, the value of T_m was determined by numerical differentiation of the experimental curve.

Nuclear Magnetic Resonance (NMR) Spectroscopy. NMR experiments were performed on Varian Instruments Inova 500 and 600 MHz spectrometers. All spectra were internally referenced to sodium 3-trimethylsilyl-2,2,3,3-d_4 propionate (TSP) at 0.0 ppm. Two-dimensional (2D) spectra were taken at 2−3 mM peptide concentration at 25 °C in 90% H_2O/10% D_2O, 10 mM phosphate, and 100 mM NaCl buffer at pH 5.4. TOCSY, NOESY, and ROESY spectra were used for assignments. A NOESY spectrum of the $NTL9_{1-39}$ peptide was also performed in D_2O buffer at pD 5.1 (uncorrected). Mixing times of 75 or 100 ms were used in the TOCSY experiments, and a mixing time of 300 ms was used in the ROESY and NOESY experiments. The deviation of the chemical shifts of the C^α protons from random coil values was calculated using the random coil chemical shifts of Wishart et al. (*37*). Native state chemical shifts for NTL9 are from Kuhlman et al. (*2*).

Determination of pK_as Using NMR. pK_as were determined by monitoring chemical shifts as a function of pH. The chemical shifts of the C^β protons on aspartate and the C^γ protons on glutamate move downfield by approximately 0.2 ppm when the carboxyl group is protonated. Data were fit to the Henderson−Hasselbalch equation to determine pK_as:

$$\delta(\text{pH}) = (\delta_{\text{base}} + \delta_{\text{acid}} \times 10^{\text{p}K-\text{pH}})/(1 + 10^{\text{p}K-\text{pH}}) \quad (2)$$

where δ is the chemical shift, δ_{base} is the chemical shift associated with the unprotonated residue, δ_{acid} is the chemical shift associated with the protonated residue, and pK is the pK_a value of the residue. Data were also fit to a modified Hill equation that assumes that there are n protons titrating simultaneously at each position:

$$\delta(\text{pH}) = [\delta_{\text{base}} + \delta_{\text{acid}} \times 10^{n(\text{p}K-\text{pH})}]/[1 + 10^{n(\text{p}K-\text{pH})}] \quad (3)$$

If the Hill coefficient (n) equals 1, this expression reduces to the simple Henderson−Hasselbalch equation. A Hill coefficient of less than 1 indicates that the titration is broader than expected for the single protonation of a noninteracting site, while a Hill coefficient of greater than 1 indicates that it is sharper. TOSCY experiments with a mixing time of 75 ms were performed at different pHs to determine the chemical shifts as a function of pH. The peaks in the 2D NMR spectra were identified starting from the assignments at pH 5.4. Chemical shift data were corrected for the pH dependence of the TSP chemical shift using the following equation

$$\delta_{\text{corr}} = \delta_{\text{obs}} - 0.019(1 + 10^{5-\text{pH}})^{-1} \quad (4)$$

Sediment Equilibrium Measurements. Experiments were performed at 25 °C for $NTL9_{1-39}$ and at 4 °C for $NTL9_{1-22}$ and $CG(1-22)GC_{ox}$ with a Beckman Optima XL-A analytical ultracentrifuge, using rotor speeds of 30 000, 40 000, and 50 000 rpm. Analyses were performed at four separate peptide concentrations (50, 100, 200, and 300 μM) for $NTL9_{1-39}$. $CG(1-22)GC_{ox}$ was examined at concentrations of 10 and 40 μM and $NTL9_{1-22}$ at 50 and 300 μM. All samples were in 100 mM NaCl buffer at pH 5.4 using 10 mM phosphate. Experiments were carried out using 12 mm path length, six-channel, charcoal-filled, Epon cells with quartz windows. Partial specific volumes and solution density were calculated using the program Sednterp (*38*). The data were globally fit with a single-species model with the

Table 1: Peptide Fragments of NTL9 Used in This Study

peptide fragment	sequence[a]
	1 10 20 30 40[b]
$NTL9_{1-22}$	NH_3-**MKVIFLKDVKGKGKKGEIKNVA**-NH_2
CG(1-22)GC	NH_3-**CGMKVIFLKDVKGKGKKGEIKNVAGC**-NH_2
$NTL9_{1-34}$	NH_3-**MKVIFLKDVKGKGKKGEIKNVADGYANNFLFKQG**-NH_2
$NTL9_{1-39}$	NH_3-**MKVIFLKDVKGKGKKGEIKNVADGYANNFLFKQGLAIEA**-NH_2

[a] NH_3 denotes a free N-terminus, and NH_2 denotes an amidated C-terminus. [b] The numbering refers to the sequence of NTL9; thus, Met is always denoted residue 1.

molecular weight treated as a fitting parameter. The HID program from the Analytical Ultracentrifugation Facility at the University of Connecticut (Storrs, CT) was used for the fitting analysis.

RESULTS AND DISCUSSION

Design of Peptide Fragments. Our previous studies of peptide fragments made use of short peptides corresponding to the individual α-helices and β-strands of NTL9 (*27*, *28*), as well as one additional peptide (residues 35−42) which was prepared to provide a model of local effects on the pK_a of Glu-38. Only the peptide corresponding to the C-terminal α-helix displayed any tendency to form structure in isolation. Not too surprisingly, the peptides corresponding to the individual β-strands were unstructured. The peptide fragments examined here are considerably larger and are designed to accomplish two goals. We wish to determine the minimum amount of the domain required to exhibit structure, and we also wish to further probe the role of local interactions (defined here as interactions involving residues close in primary sequence) on the pK_a values of the acidic residues. We prepared two peptides corresponding to the first two β-strands and intervening loop. One of these was a disulfide-cyclized variant. A third peptide, 34 residues in length, contained the β-strand−loop−β-strand unit and the first α-helix as well. The final peptide constitutes the complete split $\beta-\alpha-\beta$ module.

Structural Analysis of the β1−Loop−β2 Peptides and Characterization of Electrostatic Interactions. The first two β-strands of NTL9 are connected by a loop rich in lysines and glycines. Interestingly, the loop is not disordered but appears to be ordered in the X-ray structure of L9 and in the solution structure of the isolated N-terminal domain (*5*, *39*). The region encompassed by the first two strands and connecting loop contains several residues which appear to be involved in important electrostatic interactions in the unfolded state, including Glu-17 and Asp-8 (*28*). Analysis of a set of point mutants strongly suggests that Glu-17 is involved in electrostatic interactions in the unfolded state which significantly modulate the pH-dependent stability of NTL9 (*40*). In the native state, a cluster of lysine side chains is found close to Glu-17 and Asp-8. If the hairpin were capable of forming in isolation, this might explain the origin of the unfolded state effects.

A peptide corresponding to residues 1−22 which encompasses the entire strand−loop−strand structure was prepared to examine the tendency of this important substructure to form in isolation. The peptide is denoted $NTL9_{1-22}$ and corresponds to the region colored purple in Figure 1. The primary sequence is listed in Table 1. A second peptide was prepared which consists of residues 1−22 but with a Cys-Gly unit attached at the N-terminus and a Gly-Cys unit at the C-terminus. Formation of the disulfide between the two cysteins provides a constrained variant of the strand−loop−strand unit. The two glycines were included to avoid any potential steric problems in forming the disulfide. The oxidized version of the peptide is denoted as CG(1−22)-GC_{ox}, and its primary sequence is included in Table 1. Both $NTL9_{1-22}$ and CG(1−22)GC_{ox} have a free N-terminus and an amidated C-terminus. The same numbering system is used for all peptides. Methionine is the first residue in $NTL9_{1-22}$ and is also designated Met-1 in CG(1−22)GC_{ox} even though this peptide begins with a Cys-Gly unit.

Table 2: Data Derived from Analytical Ultracentrifugation Measurements

sample	MW[a]
$NTL9_{1-22}$[b]	
50 μM	2510 ± 330
300 μM	2610 ± 250
global	2580 ± 250
CG(1−22)GC_{ox}[b]	
10 μM	2950 ± 260
40 μM	2870 ± 210
global	2900 ± 210
$NTL9_{1-39}$[c]	
50 μM	4140 ± 880
100 μM	4060 ± 450
200 μM	4070 ± 620
300 μM	3550 ± 400
global	4350 ± 850

[a] MW calculated from global fits to data collected at 30 000, 40 000, and 50 000 rpm. [b] Measured at 4 °C. [c] Measured at 25 °C.

Analytical ultracentrifugation measurements were performed on CG(1−22)GC_{ox} to rule out the formation of intermolecular disulfides. Global analysis of data collected at three rotor speeds and two peptide concentrations (10 and 40 μM) confirmed that GC(1−22)GC_{ox} is monomeric. The analysis yielded an apparent molecular weight of 2900 ± 210 which is very close to the expected value of 2751 (Table 2). $NTL9_{1-22}$ was also examined by analytical ultracentrifugation and was found to be monomeric. Global analysis of data collected at two peptide concentrations gave an apparent molecular weight of 2580 ± 250 which is very close to the expected value of 2431. Both of the peptides appear to be unstructured as judged by far-UV CD (Figure 2). There is no increase in structure at low temperatures or in the presence of Na_2SO_4, a protein stabilizing agent that has previously been shown to stabilize the native state of intact NTL9 (*3*). Two-dimensional NMR studies are fully consistent with the

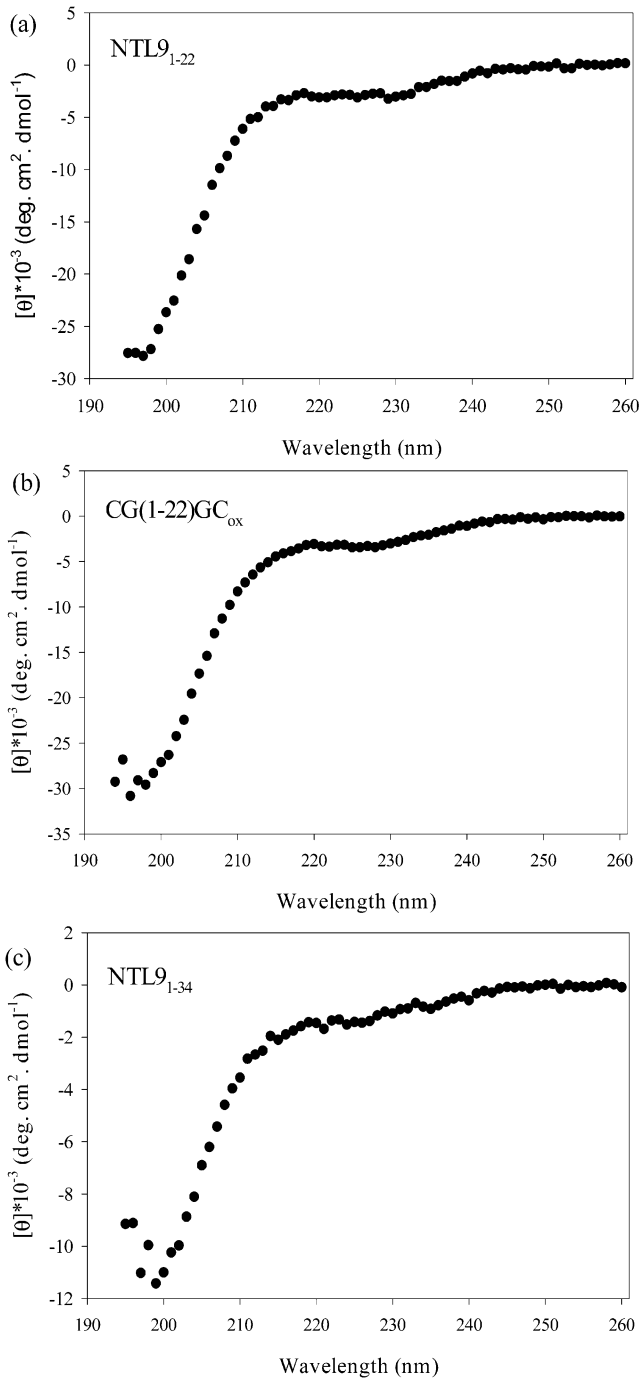

FIGURE 2: Far-UV CD spectra of (a) NTL9$_{1-22}$, (b) CG(1−22)-GC$_{ox}$, and (c) NTL9$_{1-34}$. All spectra were obtained at pH 5.4 and 25 °C.

CD experiments and confirm that both peptides are unstructured. The proton spectra of both peptides could be largely assigned using standard methods. In the native state of NTL9, cross-strand NOEs are observed between the C$^{\alpha}$ protons of residues I4 and I18, and K2 and N20. In contrast, no C$^{\alpha}$ proton−C$^{\alpha}$ proton NOEs are observed in the ROESY spectrum of either peptide. C$^{\alpha}$ proton chemical shifts are well-known to be sensitive to secondary structure, and the C$^{\alpha}$ protons of K2, V3, I4, I18, and N20 are all shifted strongly downfield of water in the native structure of NTL9. No significant deviation from random coil values was observed for either NTL9$_{1-22}$ or CG(1−22)GC$_{ox}$. Plots of the deviation from random coil values are shown in Figure

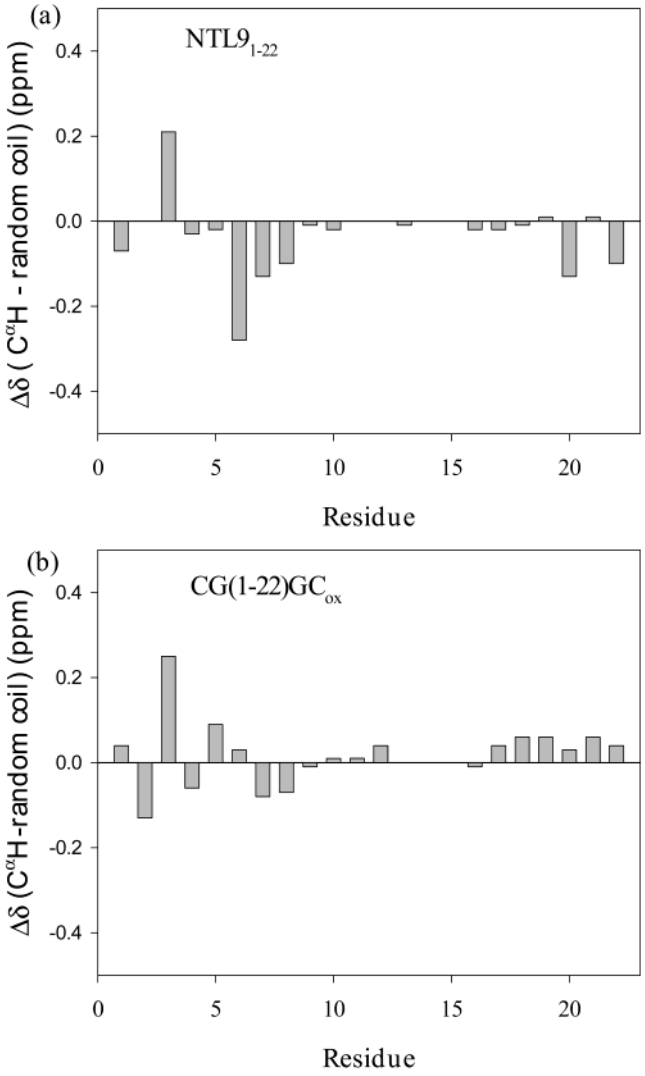

FIGURE 3: Chemical shift deviations of C$^{\alpha}$ protons between (a) NTL9$_{1-22}$ and random coil values and (b) CG(1−22)GC$_{ox}$ and random coil values.

3. The largest deviation is −0.28 ppm, while most are <0.1 ppm. In contrast, the deviations space a range of more than ±1 ppm for this region of intact NTL9 (*41*). The large deviations from the values observed for NTL9 and the small deviations of the shifts from random coil values provide good additional evidence that both peptides are unstructured.

The pK_as of Asp-8 and Glu-17 were measured for each peptide. The C$^{\beta}$ protons of Asp-8 and the C$^{\gamma}$ protons of Glu-17 shift more than 0.2 ppm downfield as the respective carboxylates are protonated. The pH-dependent shifts of these residues were followed by recording a set of TOCSY spectra from pH 7 to 2. The pK_a values were determined by fitting the data with a modified Hill equation (see Materials and Methods). The data are all well fit with Hill coefficients very close to 1, and the curves are shown in Figure 4. The pK_as of Asp-8 and Glu-17 in NTL9$_{1-22}$ are slightly lower than the values measured in smaller peptides from NTL9 but are still much larger than those measured for the folded state of NTL9. The minor shifts from the values previously measured for these groups in the fragments of residues 1−11 and 12−23 of NTL9 are consistent with the lack of structure observed by NMR and CD. The direction of the small pK_a shifts is easily understood since the fragment of residues 1−22

Table 3: pK_a Values and Hill Coefficients (n) for the Acidic Residues in NTL9 and in the Fragments of NTL9

	Asp-8		Glu-17		Glu-38	
peptide	pK_a	n	pK_a	n	pK_a	n
NTL9[a]	2.99 ± 0.05	0.94 ± 0.09	3.57 ± 0.05	0.93 ± 0.08	4.04 ± 0.05	0.95 ± 0.09
1−11[a]	3.84 ± 0.06	0.97 ± 0.08				
12−23[a]			4.11 ± 0.17	0.96 ± 0.02		
35−42[a]					4.63 ± 0.14	0.86 ± 0.20
$NTL9_{1-22}$	3.66 ± 0.04	0.98 ± 0.09	4.05 ± 0.03	0.94 ± 0.05		
$CG(1-22)GC_{ox}$	3.58 ± 0.09	1.03 ± 0.20	3.93 ± 0.03	0.93 ± 0.04		
$NTL9_{1-39}$	3.23 ± 0.06	1.12 ± 0.11	3.71 ± 0.06	1.09 ± 0.12	4.44 ± 0.03	1.28 ± 0.09

[a] The pK_a values and Hill coefficients for NTL9 are from Kuhlman et al. (*28*).

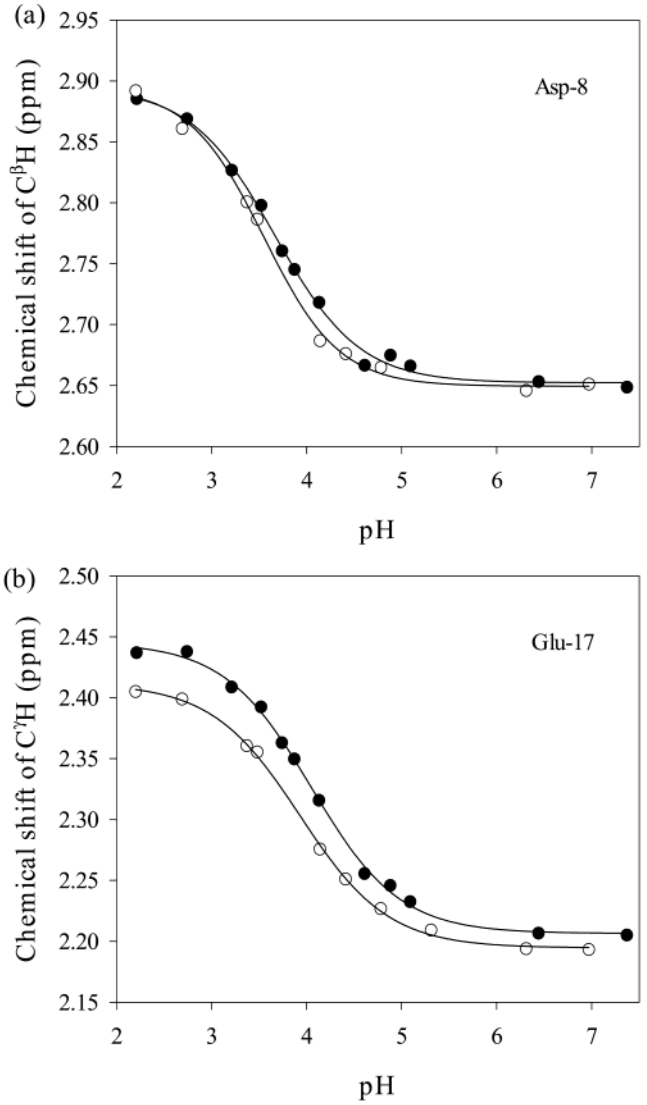

FIGURE 4: Chemical shift as a function of pH for the carboxylates in $NTL9_{1-22}$ (●) and $CG(1-22)GC_{ox}$ (○). (a) pH-dependent chemical shift of the C^{β} proton of Asp-8 and (b) pH-dependent chemical shift of the C^{γ} proton of Glu-17. The curves were fit to determine pK_a values, and solid lines represent the best fit to eq 3.

contains all of the lysines in the loop region while the shorter fragments do not. The pK_as are further shifted away from the values of residues 1−11 and 12−23 in $CG(1-22)GC_{ox}$, but the shifts are still very different from the folded state values. Again, this is consistent with the lack of structure observed for $CG(1-22)GC_{ox}$. The additional shift relative to $NTL9_{1-22}$ is also reasonable since the disulfide constraint should increase the positive charge density near Asp-8 and Glu-17. The data are summarized in Table 3.

Addition of the First Helix Is Not Sufficient To Induce Folding, but Addition of the Helix and Third Strand Is. In the intact domain, one face of the β-sheet interacts with the first α-helix to form part of the hydrophobic core in NTL9. In addition, there is an important electrostatic interaction involving the side chain of Asp-23 and the protonated N-terminus on this face of the molecule. Obviously, none of these interactions are possible in our strand−loop−strand peptides. Consequently, we prepared a larger fragment, residues 1−34, which includes the entire first helix and the residues which lead from the C-terminus of the helix to the last β-strand. The residues corresponding to the last strand are not included. We denote this construct $NTL9_{1-34}$. Far-UV CD indicates that it is unstructured. The spectrum recorded at pH 5.4 and 25 °C is displayed in Figure 2c. No additional structure is induced by lowering the temperature or by adding sulfate. Unfortunately, the unexpectedly low yield of this peptide meant that there was not enough material to conduct detailed pH titrations.

In striking contrast, the addition of just five more residues leads to a well-folded molecule. This peptide, denoted $NTL9_{1-39}$, includes the first 39 residues of NTL9 and comprises the entire three-stranded β-sheet and the first helix. It constitutes the complete split $\beta-\alpha-\beta$ motif and corresponds to the purple and green colored portion of Figure 1. The far-UV CD spectrum of this peptide is shown in Figure 5a. The strong positive maximum below 200 nm and the significant negative intensity from 205 to >230 nm are indicative of a folded structure. The spectrum is somewhat different from the published spectrum of NTL9 with less intensity in the 222 nm region (*41*). This is entirely reasonable since the additional 17 residues present in intact NTL9 form a long α-helix. $NTL9_{1-39}$ also exhibits a near-UV CD spectrum (Figure 5b) indicating that the single tyrosine (there are no tryptophans) is held in a rigid environment. This provides evidence that tertiary interactions are formed and that the molecule is not in a molten globule-like state. Fluorescence experiments indicate that the protein does not bind ANS, providing even more evidence that it populates a well-defined native state and not a molten globule.

In the native state of NTL9, one face of the β-sheet is covered by the C-terminal helix with Leu-44 and Leu-47 from the helix making contact with Ile-4, Ile-18, and Ile-37 from the sheet. In the absence of the C-terminal helix, these residues will be partially exposed to solvent. The exposed hydrophobic groups might promote self-association; thus, it is very important to establish that $NTL9_{1-39}$ is monomeric. Analytical ultracentrifugation experiments were performed at several rotor speeds and several peptide concentrations

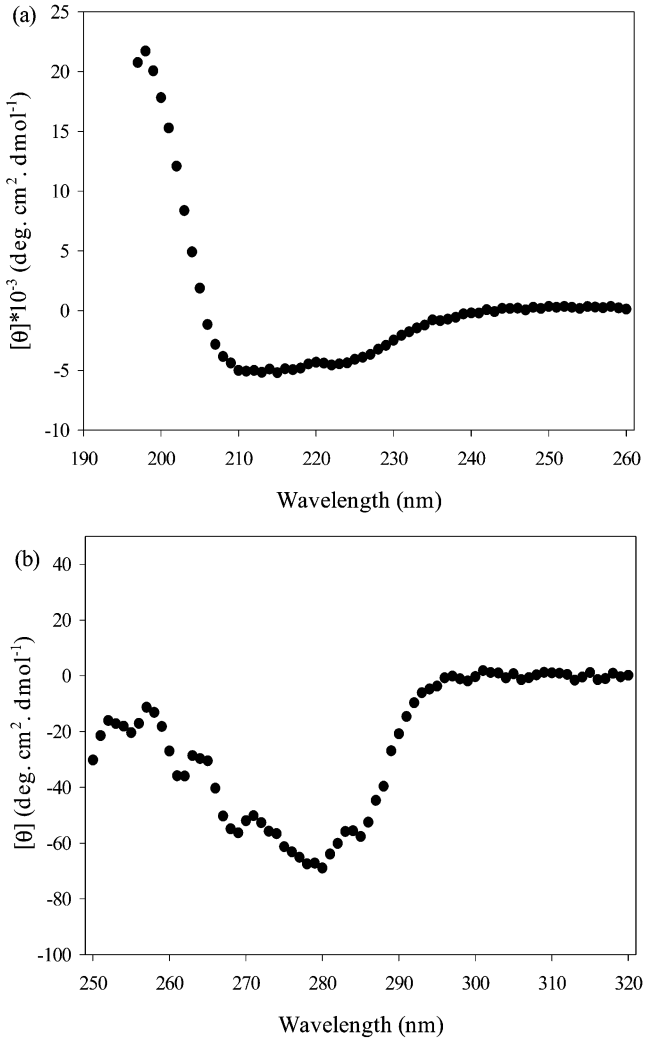

FIGURE 5: (a) Far-UV CD and (b) near-UV CD spectra of $NTL9_{1-39}$. The spectra were obtained at pH 5.4 and 25 °C.

(Table 2). Global analysis of all data sets yielded an apparent molecular weight of 4350 ± 850 which agreed very well with the expected monomer weight of 4283. In addition, there was no systematic deviation in molecular weight with changes in peptide concentration.

$NTL9_{1-39}$ Adopts Nativelike Structure. The CD and ANS fluorescence experiments demonstrate that $NTL9_{1-39}$ is well-folded, but they do not provide any detailed structural information. Fortunately, the ^{1}H NMR spectrum of this molecule is reasonably well resolved, and backbone assignments for 36 of the 39 residues could be made. The observed C^α proton chemical shifts are consistent with the global fold being very similar to that of NTL9. Strong downfield shifts are observed for C^α protons in the β-sheet just as we observed for the intact protein. The deviation of the C^α proton shifts from random coil values is compared to the deviation from the values in NTL9 in Figure 6. Deviations from random coil values are large, ranging up to ±1.2 ppm, while the deviations from the shifts measured in NTL9 are much smaller, spanning the range of only 0.07 to −0.17 ppm. More direct evidence for nativelike structure is provided by a NOESY experiment. In the intact protein, C^α proton−C^α proton NOEs are observed between I4 and I18, K2 and N20, F5 and A36, and V3 and E38. The C^α proton−C^α proton region of the NOESY spectrum of $NTL9_{1-39}$ is displayed in

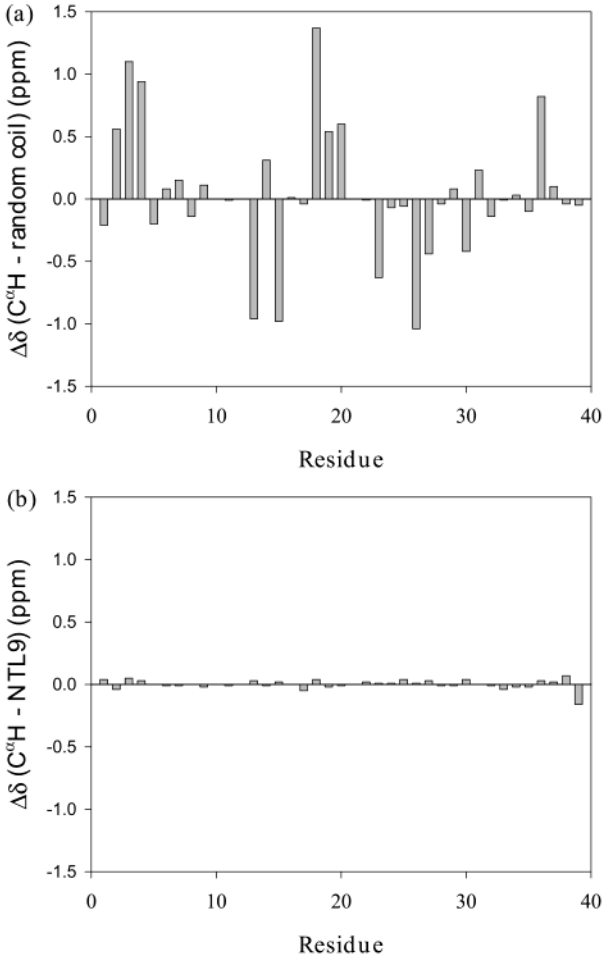

FIGURE 6: Chemical shift deviations of C^α protons of $NTL9_{1-39}$: (a) difference between $NTL9_{1-39}$ and random coil values and (b) difference between $NTL9_{1-39}$ and NTL9 values.

Figure 7. NOE cross-peaks between these C^α protons are clearly resolved. The cross-peak between K2 and N20 is weak, especially above the diagonal. This is likely due to cross-saturation of the K2 C^α proton during solvent suppression. The final piece of NMR evidence indicating a nativelike fold is the observation of ring current-shifted methyl resonances at 0.52 ppm from V3, 0.77 ppm from A26, and 0.95 ppm from A36. These peaks are observed at 0.58, 0.74, and 0.96 ppm, respectively, in intact NTL9. $NTL9_{1-39}$ has a free energy of unfolding between 1.8 and 2.0 kcal/mol; this means that up to ca. 3−5% of the peptide could be unfolded at 25 °C. We did not observe a second set of minor peaks in the spectrum. This is consistent with our previous observation that intact NTL9 folds very rapidly and is in fast exchange on the NMR time scale.

pK_a measurements provide additional, excellent evidence that $NTL9_{1-39}$ adopts a global fold very similar to that of the same region in intact NTL9. We were unable to follow resonances associated with Asp-23, but the pK_as of the three other residues (Asp-8, Glu-17, and Glu-38) could be estimated. The apparent pK_a values of Asp-8 and Glu-17 are only slightly higher than those measured in NTL9, and they are significantly lower than the values determined for the shorter peptides. The small difference between the values measured for NTL9 and $NTL9_{1-39}$ is likely due to the fact that $NTL9_{1-39}$ starts to unfold at low pH values. The unfolded state pK_as are higher than the folded state values; thus,

Table 4: Equilibrium Thermodynamic Parameters for $NTL9_{1-39}$ and Intact NTL9 Derived from Thermal Unfolding and Urea Denaturation at 25 °C and pH 5.4 with 10 mM Sodium Phosphate and 100 mM Sodium Chloride

	CD at 222 nm			fluorescence at 305 nm			thermal unfolding
protein	$\Delta G°(H_2O)$ (kcal/mol)	m (kcal mol^{-1} M^{-1})	C_M (M)	$\Delta G°(H_2O)$ (kcal/mol)	m (kcal mol^{-1} M^{-1})	C_M (M)	T_m (°C)
NTL9[a]	4.45	0.72	6.18				77.3
$NTL9_{1-39}$	1.81 ± 0.12	0.47 ± 0.02	3.87 ± 0.09	1.96 ± 0.05	0.51 ± 0.01	3.83 ± 0.04	58.0

[a] The thermodynamic parameters of NTL9 are taken from Luisi et al. (*1*).

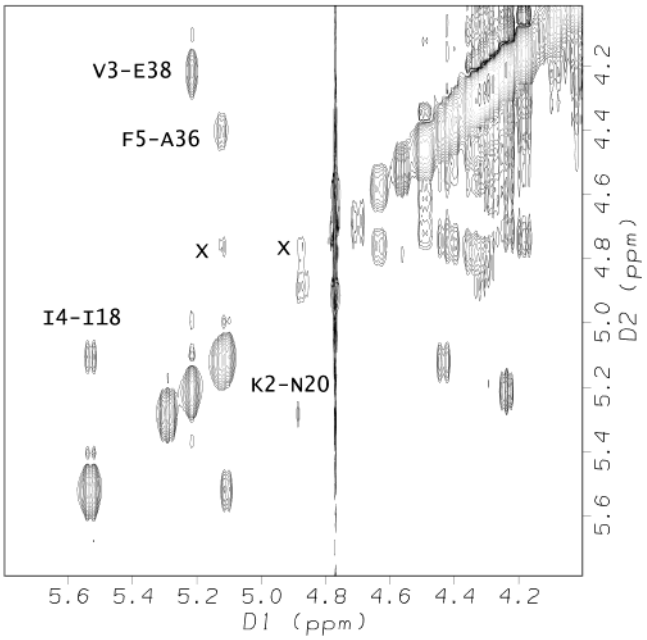

FIGURE 7: Portion of the 2D NOESY spectrum of $NTL9_{1-39}$ in D_2O at 25 °C and pD 5.1 (uncorrected). NOEs between C^α protons on adjacent β-strands are labeled. Artifacts resulting from residual HOD in the D2 dimension are labeled with an X.

unfolding at the lower-pH limits will lead to a systematic error and an overestimation of the pK_a values. The Hill coefficients for the $NTL9_{1-39}$ Asp-8 and Glu-17 titrations are slightly different from unity, and this is also an effect of the low-pH unfolding. The apparent pK_a of Glu-38 in $NTL9_{1-39}$ is very similar to that measured in a small peptide and is higher than the value found in NTL9. This is reasonable since Glu-38 is at the C-terminus of $NTL9_{1-39}$ and hence is in a very different environment in $NTL9_{1-39}$ and NTL9. The results of the pK_a determination are listed in Table 3.

$NTL9_{1-39}$ Folds Cooperatively. Cooperative folding and unfolding is a hallmark of natural globular proteins; in contrast, many designed proteins and some small natural polypeptides exhibit diffuse unfolding transitions. Urea denaturation experiments were conducted to estimate the stability of $NTL9_{1-39}$ and to test the cooperativity of the unfolding. The unfolding curve is displayed in Figure 8a and shows the characteristic sigmoidal shape expected for a well-folded protein, and more importantly, the curves monitored by fluorescence and by far-UV−CD overlap. As expected, $NTL9_{1-39}$ is less stable than NTL9. The midpoint of the urea denaturation is 3.87 M urea for $NTL9_{1-39}$ and 6.18 M for intact NTL9. The m value of $NTL9_{1-39}$ is 0.47 kcal mol^{-1} M^{-1}, which is smaller than the value measured for NTL9 under similar conditions (0.72 kcal mol^{-1} M^{-1}). m values are related to the change in buried surface area between the

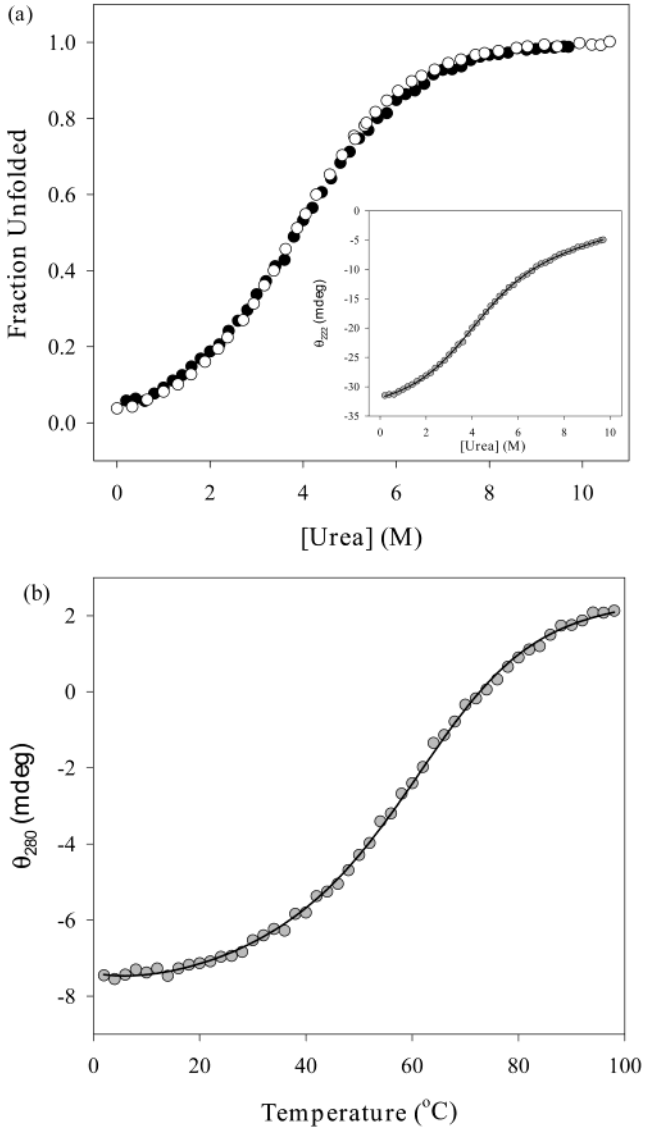

FIGURE 8: (a) Urea-induced unfolding of $NTL9_{1-39}$ followed by CD measurements at 222 nm (●) and fluorescence at 305 nm (○). Both measurements were performed at pH 5.4 and 25 °C, and the unfolded fraction was calculated as described in Materials and Methods. The inset shows the data for the CD-monitored denaturation. (b) Thermal unfolding curve of $NTL9_{1-39}$. The solid lines indicate the fits.

folded state and the unfolded state. The reduction in the m value is expected, and the measured m value is consistent with empirical correlations that relate the m value to the size of globular proteins (*42*). $\Delta G°$ of unfolding in the absence of urea is calculated to be between 1.8 and 2.0 kcal/mol, and again the value is smaller than that measured for the intact domain under similar conditions. There are a number of examples of designed proteins and partially folded states of natural proteins (molten globules), which display sigmoi-

dal unfolding curves for denaturant-induced unfolding but which show diffuse thermal unfolding curves. In contrast to these poorly folded systems, $NTL9_{1-39}$ exhibits a sigmoidal thermal unfolding curve. The CD-monitored thermal denaturation is shown in Figure 8b. The midpoint of unfolding is near 58 °C which is lower than that measured for NTL9 but is still relatively high. The width of the transition is consistent with the small size of $NTL9_{1-39}$. The stability data are summarized in Table 4. The previously determined values for NTL9 are included for comparison.

CONCLUSION

Our analysis of NTL9 shows that the entire split $\beta-\alpha-\beta$ motif is the minimum unit required for cooperative folding. The smaller fragments characterized here, although containing significant portions of the $\beta-\alpha-\beta$ unit, are unstructured even in the presence of stabilizing agents or even when constrained by introduced disulfides that are designed to favor nativelike topology. The studies of the smaller fragments have important implications for studies of the unfolded state of NTL9, while our characterization of $NTL9_{1-39}$ adds another member, with a unique fold, to the small number of cooperatively folded "miniature" proteins.

Previous studies have indicated that there are significant electrostatic interactions in the unfolded state of NTL9. That work used short peptide fragments to provide model unfolded state pK_a values for the six acidic residues in NTL9 (*28*). The fragments were chosen in an attempt to capture local sequence effects on unfolded state pK_a values. One potential cause for concern is that the fragments might not be good models for local sequence effects. If this were the case, then the interpretation of the pH-dependent stability data might need to be revised. Perhaps the most worrisome residues in this regard are Asp-8 and Glu-17 since they are N-terminal and C-terminal, respectively, to the lysine glycine rich loop and the intact loop was not included in the previous set of fragments. The analysis presented for the $NTL9_{1-22}$ and $CG(1-22)GC_{ox}$ peptides strongly argues that this is not a problem since the pK_a values of the acidic residues in these constructs are very similar to the values observed in the shorter fragments. In addition, the pK_a values measured for $NTL9_{1-22}$ and $CG(1-22)GC_{ox}$ combined with the structural analysis provide evidence that any strong propensity to form structure in this region in isolation cannot account for the unfolded state interactions inferred for NTL9.

To the best of our knowledge, the work reported here is the first demonstration of the cooperative folding of an isolated split $\beta-\alpha-\beta$ unit. Removal of the C-terminal helix of NTL9 to generate $NTL9_{1-39}$ leaves an exposed hydrophobic patch made up of residues from the three-stranded β-sheet, but the native state structure does provide clues as to why $NTL9_{1-39}$ is still able to fold. Ile-37 and Ala-39 on the third strand, Ile-4 and Leu-6 on the first strand, and Ile-18 on the second strand are each partially exposed to solvent upon removal of the helix. These residues form significant interactions with each other in addition to their interactions with the helix. In particular, Ile-4 and Ile-18 have significant mutual interactions while Ile-4 also packs against Ile-37, which in turn interacts with Leu-6. Ala-39 and Ile-18 are on the outermost strands of the sheet (the topology is 1, $-2X$), and the twist of the sheet allows them to pack against each other. This network of side chain interactions leads to numerous van der Waals contacts and also shields the backbone hydrogen bonds in the sheet from solvent. The stability of the domain is modest with an estimated $\Delta G°$ of 1.8−2.0 kcal/mol at 25 °C and a T_m of 58 °C. Small proteins normally have high T_ms because their small size means that the changes in heat capacity and entropy of unfolding are small (*16*, *43*). $\Delta S°$ is directly related to the slope of the $\Delta G°$ versus T plot, while the curvature is related to $\Delta C_p°/T$; thus, small proteins normally have shallow Gibbs−Helmholtz profiles, and their high T_ms do not imply a large value of $\Delta G°$ at any temperature. The relatively high T_m and the modest $\Delta G°$ for $NTL9_{1-39}$ are consistent with these observations. The stabilities of three other naturally occurring cooperatively folded structures of ≤40 residues have been reported. The free energy of unfolding and the T_ms of all four of these small proteins are very similar. Two of the other proteins, the 36-residue villin subdomain and the 41-residue peripheral subunit-binding domain, are all helical structures. The free energy of unfolding of the villin headpiece subdomain has been estimated to be 3.1 kcal/mol at 4 °C, and the T_m equals 70 °C. The $\Delta G°$ of unfolding for the peripheral subunit-binding domain was also found to be 3.1 kcal/mol at 4 °C and is 2.2 kcal/mol at 25 °C. The T_m for this domain is 53 °C. A 36-residue version of the peripheral subunit-binding domain is only slightly less stable with a $\Delta G°$ for unfolding of 1.8 kcal/mol at 25 °C and a T_m of 48 °C. A 34-residue version of the all β-sheet Pin 1 WW domain (36 residues if two additional residues resulting from the expression systems are counted) folds cooperatively with an estimated $\Delta G°$ of unfolding of 3.3 kcal/mol at 4 °C and a T_m of 58 °C (*44*).

It is natural to inquire if there is something unusual about these small domains which allows them to fold cooperatively. Limited data are available, but in our view, the answer appears to be no. Early work based on the measured per residue values of standard thermodynamic parameters suggested that the minimum size of a cooperatively folded structure would need to be on the order of 50 residues (*45*). The existence of smaller cooperatively folded units does not necessarily mean these predictions are incorrect or that unusual features are required to maintain small folded structures. It is important to recall that the early analysis attempted to predict the minimum size required for a protein to have a $\Delta G°$ significantly larger than random thermal energy, RT, at or above room temperature. In fact, the small proteins analyzed to date, including $NTL9_{1-39}$, have $\Delta G°$ values at 25 °C which are only several times greater than RT. In addition, all of these domains are part of larger structures and/or function to bind ligands; thus, they may well be more stable in their biologically relevant context. A detailed thermodynamic analysis has been reported for only one miniature protein, the peripheral subunit-binding domain. Importantly, that study showed that the per residue values of $\Delta H°$ and $\Delta C_p°$ all fell within the normal range for globular single-domain proteins, indicating that there was nothing unusual about the thermodynamics of its folding (*16*). Recent work has highlighted aromatic−aromatic interactions and aromatic−proline interactions as potential mechanisms for stabilizing small proteins. For example, the villin headpiece subdomain contains an interesting cluster of buried aromatic residues, while a small designed β-hairpin appears to rely

on Trp−Trp contacts for stability (*46*). Aromatic−proline interactions are also thought to play a role in stabilizing some unusually small cooperatively folded structures (*12*, *17*). None of these interactions are present in $NTL9_{1-39}$ or for that matter in the peripheral subunit-binding domain; thus, while they might provide one means of stabilizing a cooperative fold, they are clearly not the only way.

ACKNOWLEDGMENT

We thank Dr. Yuxin Hua for his contributions to the early stages of this work.

REFERENCES

1. Luisi, D. L., and Raleigh, D. P. (2000) *J. Mol. Biol. 299*, 1091−1100.
2. Kuhlman, B., Boice, J. A., Fairman, R., and Raleigh, D. P. (1998) *Biochemistry 37*, 1025−1032.
3. Kuhlman, B., Luisi, D. L., Evans, P. A., and Raleigh, D. P. (1998) *J. Mol. Biol. 284*, 1661−1670.
4. Lillemoen, J., Cameron, C. S., and Hoffman, D. W. (1997) *J. Mol. Biol. 268*, 482−493.
5. Hoffman, D. W., Davies, C., Gerchman, S. E., Kycia, J. H., Porter, S. J., White, S. W., and Ramakrishnan, V. (1994) *EMBO J. 13*, 205−212.
6. Hoffman, D. W., Cameron, C. S., Davies, C., White, S. W., and Ramakrishnan, V. (1996) *J. Mol. Biol. 264*, 1058−1071.
7. Orengo, C. A., and Thornton, J. M. (1993) *Structure 1*, 105−120.
8. Efimov, A. V. (1994) *FEBS Lett. 355*, 213−219.
9. Efimov, A. V. (1995) *J. Mol. Biol. 245*, 402−415.
10. Lopez de la Paz, M., Lacroix, E., Ramirez-Alvarado, M., and Serrano, L. (2001) *J. Mol. Biol. 312*, 229−246.
11. Hill, R. B., Raleigh, D. P., Lombardi, A., and DeGrado, W. F. (2000) *Acc. Chem. Res. 33*, 745−754.
12. Gellman, S. H., and Woolfson, D. N. (2002) *Nat. Struct. Biol. 9*, 408−410.
13. Ottesen, J. J., and Imperiali, B. (2001) *Nat. Struct. Biol. 8*, 535−539.
14. Pokala, N., and Handel, T. M. (2001) *J. Struct. Biol. 134*, 269−281.
15. Spector, S., Kuhlman, B., Fairman, R., Wong, E., Boice, J. A., and Raleigh, D. P. (1998) *J. Mol. Biol. 276*, 479−489.
16. Spector, S., Young, P., and Raleigh, D. P. (1999) *Biochemistry 38*, 4128−4136.
17. Neidigh, J. W., Fesinmeyer, R. M., and Andersen, N. H. (2002) *Nat. Struct. Biol. 9*, 425−430.
18. Duan, Y., Wang, L., and Kollman, P. A. (1998) *Proc. Natl. Acad. Sci. U.S.A. 95*, 9897−9902.
19. Duan, Y., and Kollman, P. A. (1998) *Science 282*, 740−744.
20. Mayor, U., Johnson, C. M., Daggett, V., and Fersht, A. R. (2000) *Proc. Natl. Acad. Sci. U.S.A. 97*, 13518−13522.
21. Chin, J. W., and Schepartz, A. J. (2001) *J. Am. Chem. Soc. 123*, 2929−2930.
22. Mer, G., Kellenberger, E., and Lefevre, J.-F. (1998) *J. Mol. Biol. 281*, 235−240.
23. DeGrado, W. F., and Sosnick, T. R. (1996) *Proc. Natl. Acad. Sci. U.S.A. 93*, 5680−5681.
24. Koepf, E. K., Petrass, Sudol, M., and Kelly, J. W. (1999) *Protein Sci. 8*, 841−853.
25. Hansen, K. C., Rock, R. S., Larsen, R. W., and Chan, S. (2000) *J. Am. Chem. Soc. 122*, 11567−11568.
26. Munoz, V., Thompson, P. A., Hofrichter, J., and Eaton, W. A. (1997) *Nature 390*, 196−199.
27. Luisi, D. L., Wu, W. J., and Raleigh, D. P. (1999) *J. Mol. Biol. 287*, 395−407.
28. Kuhlman, B., Luisi, D. L., Young, P., and Raleigh, D. P. (1999) *Biochemistry 38*, 4896−4903.
29. Shortle, D. (1996) *FASEB J. 10*, 27−34.
30. Neira, J. L., and Fersht, A. R. (1999) *J. Mol. Biol. 285*, 1309−1333.
31. Oliveberg, M., Arcus, V., and Fersht, A. R. (1995) *Biochemistry 34*, 9424−9433.
32. Swint-Kruse, L., and Robertson, A. D. (1995) *Biochemistry 34*, 4724−4732.
33. Tanford, C. (1970) *Adv. Protein Chem. 24*, 1−95.
34. Tan, Y.-J., Oliverberg, M., Davis, B., and Fersht, A. R. (1995) *J. Mol. Biol. 254*, 980−992.
35. Pace, C. N., Vajdos, F., Fee, L., Grimsley, G., and Gray, T. (1995) *Protein Sci. 4*, 2411−2423.
36. Pace, C. N. (1986) *Methods Enzymol. 131*, 266−280.
37. Wishart, D. S., and Sykes, B. D. (1994) *Methods Enzymol. 239*, 363−392.
38. Laue, T., Shaw, B. D., Ridgeway, T. M., and Pelletier, S. L. (1992) in *Analytical Ultracentrifugation in Biochemistry and Polymer Science* (Harding, S. E., Rowe, A. J., and Horton, J. C., Eds.) pp 90−125, The Royal Society of Chemistry, Cambridge, United Kingdom.
39. Hua, Y. (1999) Ph.D. Thesis, Department of Chemistry, State University of New York at Stony Brook, Stony Brook, NY.
40. Luisi, D. L. (2000) Ph.D. Thesis, Department of Chemistry, State University of New York at Stony Brook, Stony Brook, NY.
41. Luisi, D. L., Kuhlman, B., Sideras, K., Evans, P. A., and Raleigh, D. P. (1999) *J. Mol. Biol. 289*, 167−174.
42. Myers, J. K., Pace, C. N., and Scholtz, J. M. (1995) *Protein Sci. 4*, 2138−2148.
43. Alexander, P., Fahnestock, S., Lee, T., Orban, J., and Bryan, P. (1992) *Biochemistry 31*, 3597−3603.
44. Kaul, R., Angeles, A. R., Jager, M., Powers, E. T., and Kelly, J. W. (2001) *J. Am. Chem. Soc. 123*, 5206−5212.
45. Privalov, P. L. (1989) *Annu. Rev. Biophys. Biophys. Chem. 18*, 47−69.
46. Cochran, A. G., Skelton, N. J., and Starovasnik, M. A. (2001) *Proc. Natl. Acad. Sci. U.S.A. 98*, 5578−5583.
47. Kraulis, P. J. (1991) *J. Appl. Crystallogr. 24*, 946−950.

BI026410C